CLAS-NOTE 2005-012
August 8 2005

Energy calibration of the Hall B bremsstrahlung tagging system using a magnetic pair spectrometer.

S. Stepanyan, B. Mecking, L. Guo, D. Dale, I. Nakagawa,
A. Teymurazyan, M. Gabrielyan, M. Wood, A. Glamazdin

1 Introduction

During the search for pentaquarks in the `g2a` data it, was found that the photon energy as defined by the tagging system [1], E_{tagg}, is different from the photon energy reconstructed in CLAS. The neutron mass was used as a constraint in the kinematically complete reaction $\gamma d \to p\pi^+\pi^-(n)$ to calculate photon energy, E_γ [3]. The shape of the dependence of the ratio of these two energies on the tagger E-counter position suggested a possible sagging of the frames that hold the E-counters. There was corroborating evidence from simulations of the effects of gravitational sag and various possible misalignments of the tagger focal plane [2]. The scale of the relative energy shifts between the `E`-counters was found to be $\sim 0.5\%$.

During the `g10` run, special measurements are carried out to determine the relative energy shifts of the tagger E-counters independent of CLAS. The tagged photon energy spectrum was measured in coincidence with e^+e^- pairs detected in the Hall-B pair spectrometer (PS) at several different values of the PS dipole field. As a correction factor the ratio of the photon energy measured in the pair spectrometer (determined by using a simplified model for the e^+e^- momentum reconstruction $E^c_\gamma = E_{e^+} + E_{e^-}$) to the energy reported by the tagging system, E_{tagg}, is defined. The aim was to have these ratios determined at the level of $\sim 10^{-3}$. For these measurements the PS was instrumented with additional the micro-strip detectors, to get better position determination of e^+ and e^-, and thus better energy resolution.

In this note, the analysis of the data collected during the special measurements for the tagger energy calibration is presented. In addition to the relative energy calibration, the method used in this analysis allows to define the absolute energy scale using special measurements with PS settings close to the end-point energy. Correction coefficients are derived for each

E-counter. The accuracy of this method is estimated to be $\pm 0.1\%$.

2 Experimental setup and the measurements

A schematic view of the setup is shown in Figure 1. The Hall B photon beam is produced in the interaction of the primary electron beam with the "Radiator" (10^{-4}r.l.), located upstream of the tagger dipole magnet. The primary electron beam gets deflected in the magnetic field of the tagger magnet to the beam dump, while electrons that loose 0.2 to 0.95 of their energy get detected in the tagger hodoscope (tagged photon energy range is from 0.2 to $0.95E_o$). The Hall B pair spectrometer (PS) is located $\sim$ 10m downstream of the "Radiator". PS consists of a dipole magnet and two planes of scintillation counters, PS1 and PS2, positioned symmetrically on the beam direction. The pair production converter is located 55.77 cm upstream of the PS dipole center and is 10^{-3}r.l. thick. For this measurement, in addition to the scintillator detectors, PS was instrumented with two pairs of micro-strip detectors (MS) that provide better position determination for the e^+e^- after the dipole. Each pair of MS detectors covers $20 \times 20\text{mm}^2$ detection area and consists of X and Y planes. The pitch size of the MS planes is $50\mu m$. MS is located at 930.70 cm downstream of the magnet center. The distance between the centroids of the "X" planes was 450 ± 0.5mm, centered on the beam axis. The beam centerline and the centers of the MS detectors were forming a plane that was approximately the mid-plane of the PS dipole.

A coincidence signal from the scintillator counters was used to trigger the DAQ system. For each triggered event, information from the tagger E- and T-counters, and from the X, Y planes of the MS were recorded. Information on beam current, beam position, and magnetic field settings was recorded as well.

The measurements were conducted for several settings of the PS dipole field in the range from -1.3T to -0.36T (currents from -2278A to -543A). At these field values, the sum of the energies of the detected e^+e^- covers almost the full range of the tagged photon spectrum. The PS magnetic field value was measured with a Hall probe ("Lake Shore" Gaussmeter) positioned in the center of the magnet. The accuracy of the device in the range of the measured fields is a few $\times 10^{-4}$. The whole data taking process was automated. At each field setting, data were acquired for 15 min of real beam time. A total of about 180 settings of the PS field were measured.

For the determination of the absolute energy scale, one run was taken at PS B-field values from -1.9T to -1.35T (currents from -2775A to -2073A), the "end point" measurements. At these values of the field, the sum of e^+ and e^- energies should be close to the endpoint of the bremsstrahlung spectrum. Measurements of the e^+e^- coincidence rate at fixed geometry of the detectors allowed to relate the PS field values to the electron beam energy.

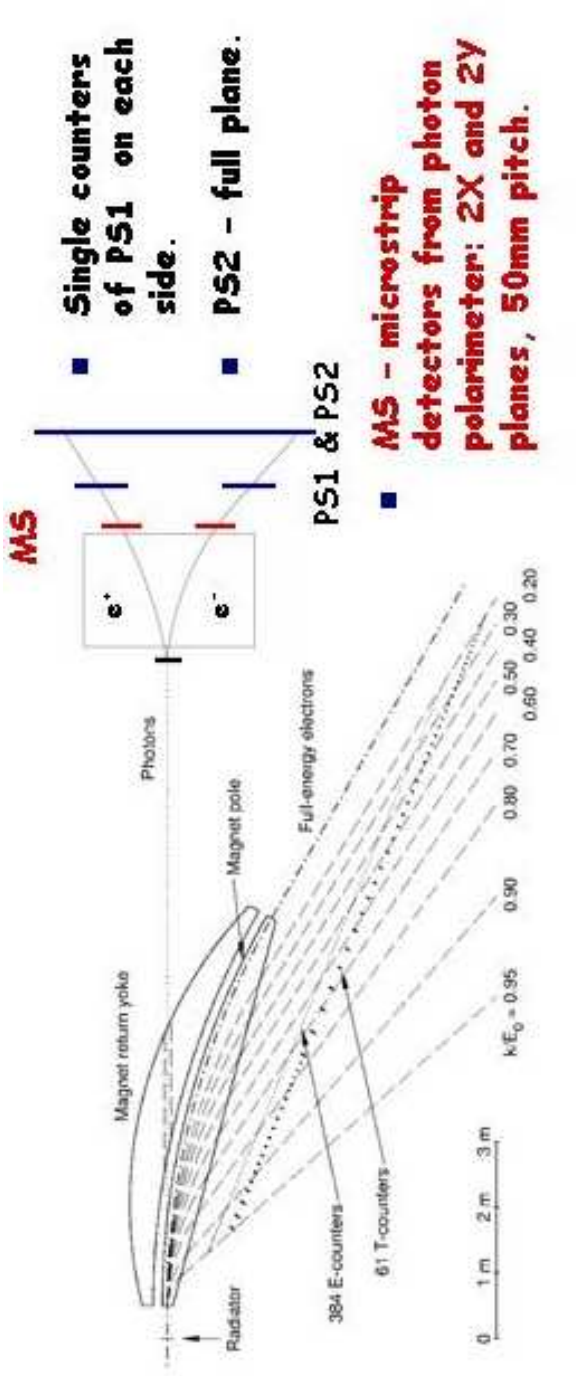

Figure 1: Hall-B tagger and PS setup.

3 Data analysis

For the data analysis standard CLAS software tools have been used. A set of new routines were added to the "ana" package to read information from the micro-strip detectors (flash ADC's), define pedestals, subtract them, and fill the ntuple. Ntuples are created with information needed for this analysis as shown in Table 1, and were filled on an event-by-event basis. For each raw BOS file one ntuple file was created.

Table 1: Structure of the Ntuple 77.

#	Bank	Variable	Comment
1	EPICS	run	Run number
2	EPICS	event	Event number in the run
3	EPICS	evntime	Event time
4	EPICS	x2c21a	X coordinate on 2C21A BPM
5	EPICS	y2c21a	Y coordinate on 2C21A BPM
6	EPICS	c2c21a	Current measured on 2c21A
7	EPICS	x2c24a	X coordinate on 2C24A BPM
8	EPICS	y2c24a	Y coordinate on 2C24A BPM
9	EPICS	c2c24a	Current measured on 2c24A
10	EPICS	pscurrent	Current of the PS dipole
11	EPICS	psprobe	PS dipole Hall probe reading
12	EPICS	taggercurrent	Current on tagger dipole
13	EPICS	taggerprobe	Tagger Hall probe reading
1	TAGR	nphot_tagr	Number hits in the tagger
2	TAGR	tagr_E_gamma(nphot_tagr)	Photon energy
3	TAGR	tagr_ttag(nphot_tagr)	Photon time
4	TAGR	tagr_tpho(nphot_tagr)	Photon time
5	TAGR	tagr_stat(nphot_tagr)	Status word (7 and 15 are OK)
6	TAGR	tagr_Tid(nphot_tagr)	T-counter ID
7	TAGR	tagr_Eid(nphot_tagr)	E-counter ID
1	MSD	nmsd	Number of hits in MSD
2	MSD	msdpl(nmsd)	MSD plane number
3	MSD	msdid(nmsd)	ID of the segment
4	MSD	msdadc(nmsd)	ADC value

Ntuple (#77) has three sub-blocks: 1) "EPICS" - information from the

EPICS and HEAD banks. 2) "TAGR" - stores reconstructed tagger hits from the TAGR bank. 3) "MSD" - stores information from microstrip detector.

3.1 Analysis of the tagger information

The standard software package for the analysis of the tagger information was used. From many reconstructed tagger hits, only hits that had status 7 or 15 were selected. Then a cut on the tagger time was applied to select hits that came withing 15 ns (-17 ns to -2 ns) relative to the trigger, see Figure 2. In Figure 3, the PS field value vs. tagger energy, E_{tagg}, is shown for the full range of measurements. The measurements cover the full photon energy range of the `g10` experiment.

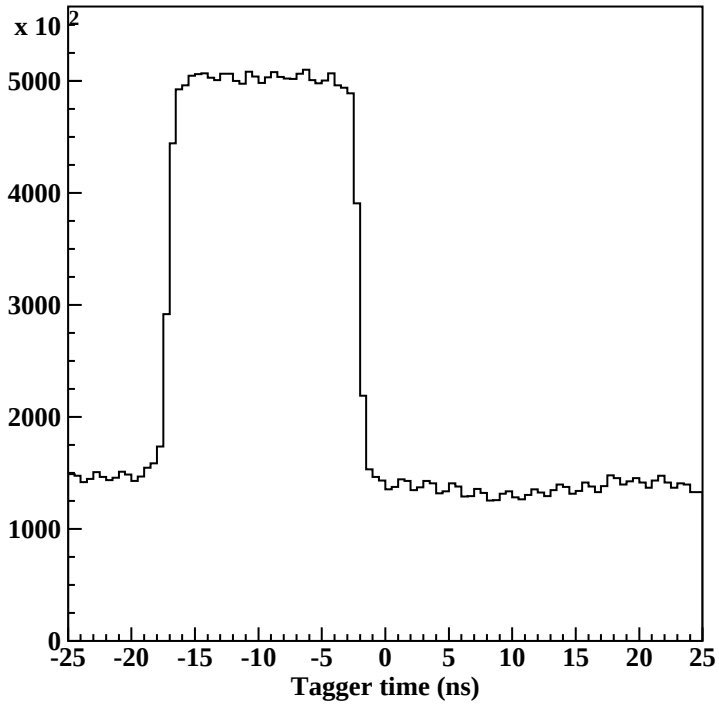

Figure 2: Tagger time distribution.

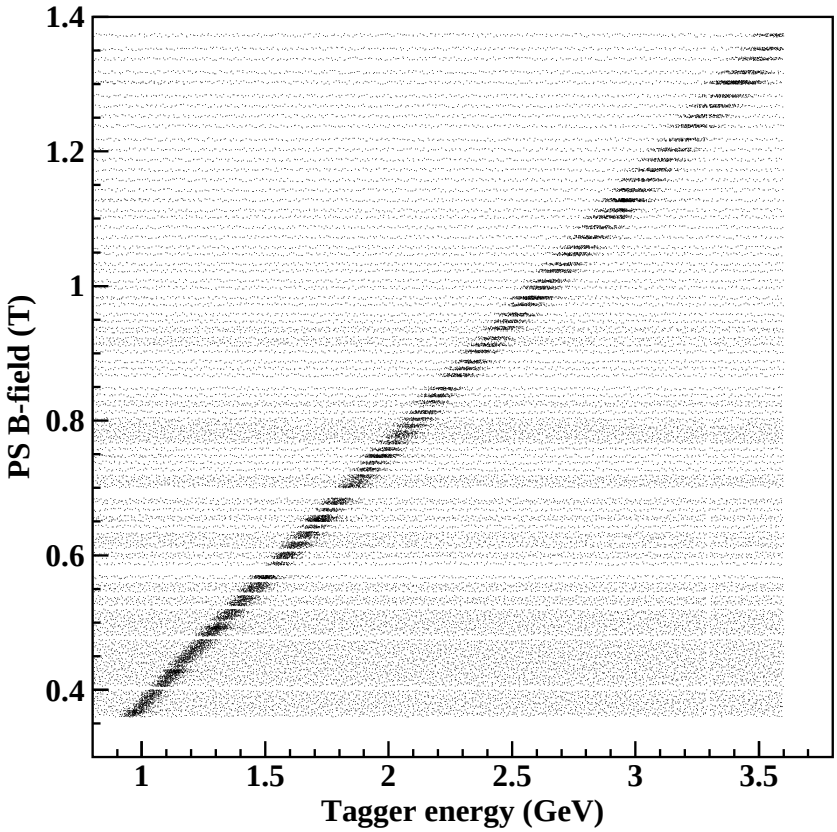

Figure 3: B-field vs tagger energy.

3.2 Analysis of the MS information

For each triggered event, several hits (ADC value above the pedestal) in the MS have been recorded. In Figure 4, the distribution of the number of hits vs. the MS plane number is shown. One of the Y planes (4) did not work. Events with more than 3 hits in any of the planes were rejected (only a small fraction of the data). For the final analysis, events with 2 or 3 hits in a plane were accepted if 2 of these hits were adjacent (adjacent hits are named a group). In Figure 5, for each of the working planes, X1, Y1, and X2, the number of found groups is plotted vs. the number of hits. If there are 2 hits (in the histogram, this bin is centered at 2.5), then the number of allowed groups is 1. If the number of reconstructed hits is 3, then the allowed number of groups can be 1 or 2. In the last case, a 2-hit group is selected as a real hit. For adjacent hits the position on the plane is calculated as a

weighted average using the ADC values (see Figure 6):

$$\overline{x} = \frac{\sum x_i \cdot ADC_i}{\sum ADC_i} \tag{1}$$

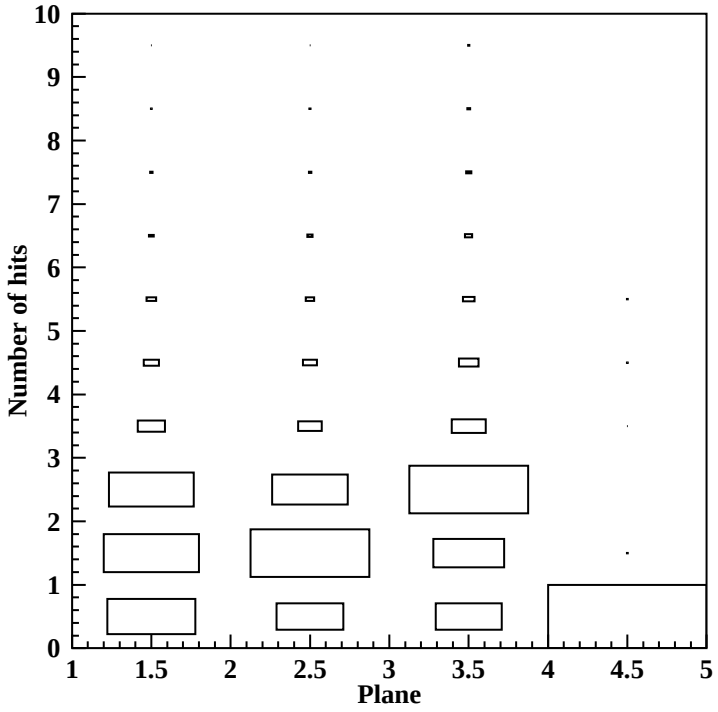

Figure 4: Distribution of number of hits for each plane.

To minimize uncertainties, the e^+e^- scattering plane was limited to be around the detector midplane by imposing a cut on the single working Y plane. In Figure 7, the distribution of hits on the working Y plane is shown. It peaks at the center of the MS plane, XZ-plane, where Z is the beam direction. Cut on the Y from pitch ID 140 to 240 was used to select e^+e^- pairs scattered in the midplane of the pair spectrometer. The distance between the e^+ and e^- in the scattering plane is shown in Figure 8. In the calculation of the photon energy, a correction is implemented (as a function of this distance) to compensate for the finite detector sizes.

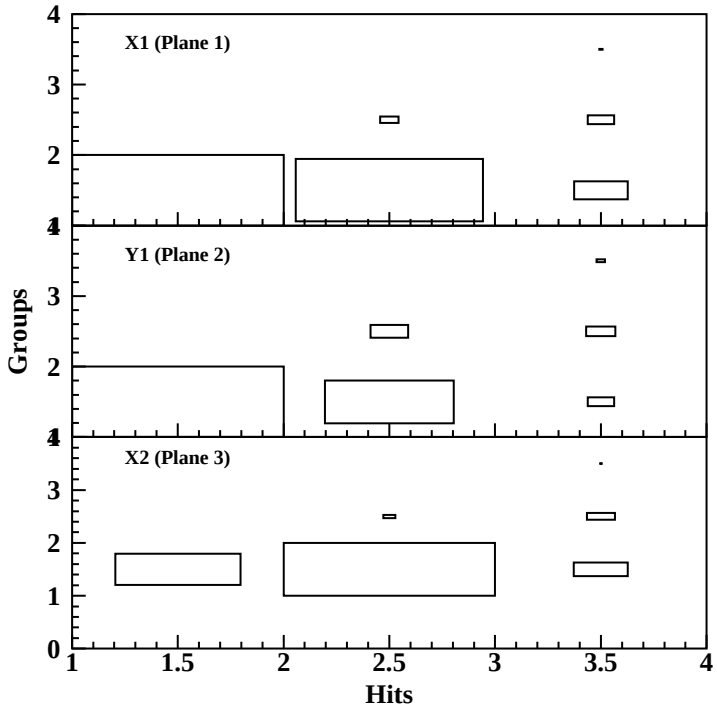

Figure 5: Distribution of hits.

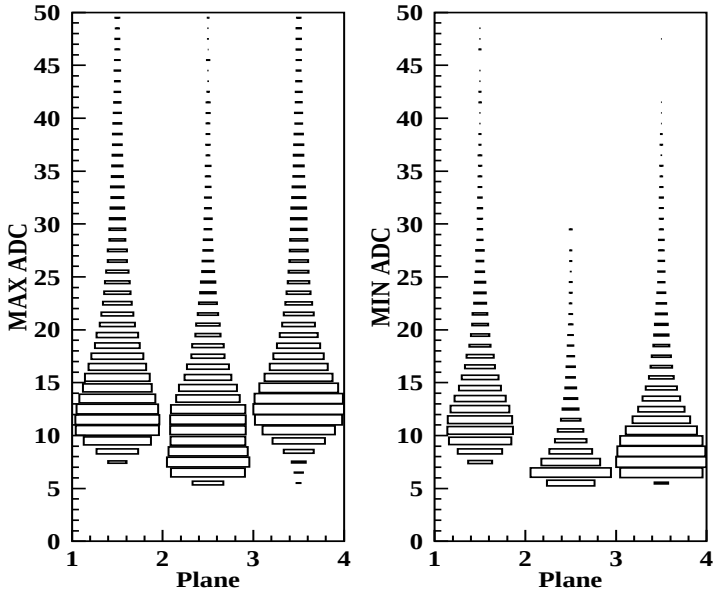

Figure 6: ADC spectra for different planes. Left panel: distribution of highest ADC values, right panel: distribution of lowest ADC values.

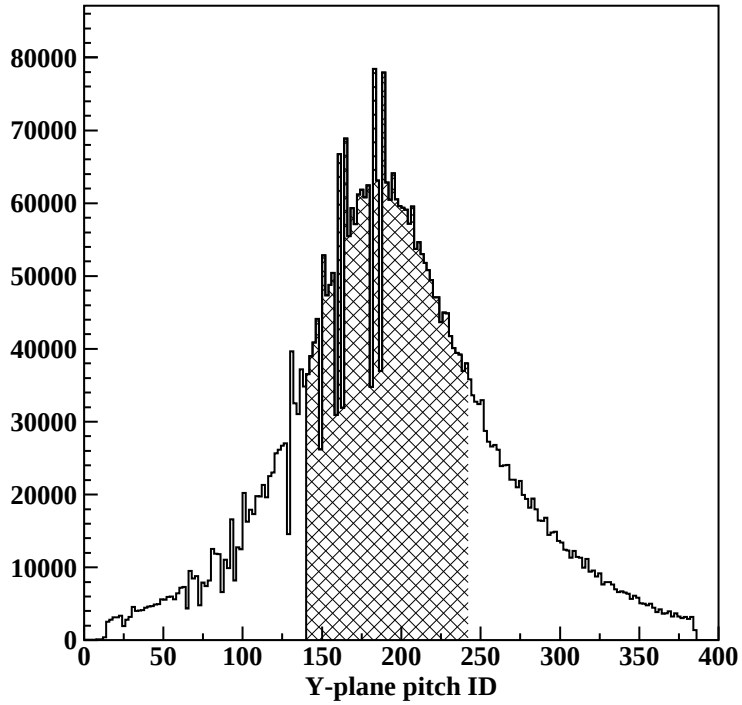

Figure 7: Distribution of hits in the Y plane.

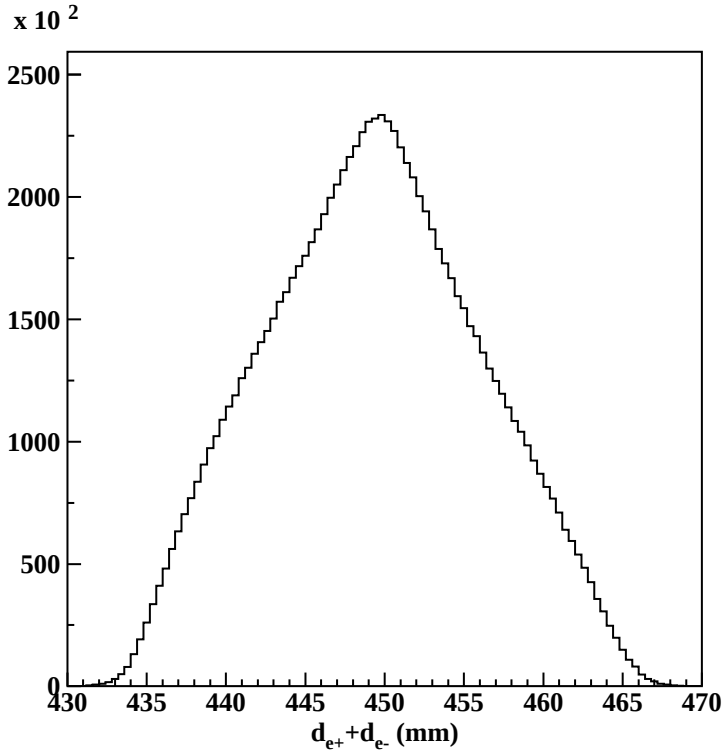

Figure 8: Distribution of the distance between e^+ and e^- in the horizontal (X) plane.

4 Tagger energy corrections

We define the average ratio of the photon energies, calculated using the PS information, and corresponding to an E-counter "i", $C_i = \overline{E^c_\gamma / E^i_{tagg}}$, as a relative energy correction for that E-counter. The information from the PS contains the momenta of e^+e^- pairs produced by a photon tagged in the E-counter "i". This ratio is calculated on an event-by-event basis for each E-counter that is within the acceptance range of the PS at a given field setting. The method assumes a simple linear relationship between the calculated and the true value of the photon energy, $E^c_\gamma = \eta \times E_\gamma$, where η does not depend on energy (or field value).

E^c_γ is defined as a sum of the e^+ and e^- momenta calculated using the reconstructed trajectories of the lepton pair and the PS dipole field value, B, measured at the center of the magnet. A simple approximation of the real field distribution by an uniform field of strength B and effective length L_{eff}, centered at the geometrical center of the magnet is assumed (see Figure 9).

$$E_\gamma \;=\; 0.2997925 \cdot (R_{e^+} + R_{e^-}) \cdot B \cdot G(d_{e^+}, d_{e^-}) \cdot F(B) \qquad (2)$$

Here the radius of the curvature $R_{e^+(e^-)}$ defined as:

$$R_{e^+(e^-)} = L_{eff}(B) \cdot \sqrt{(\frac{l_p}{d_{e^+(e^-)}})^2 + 1.} \qquad (3)$$

where l_p is the distance from the magnet center to the detector plane, and $d_{e^+(e^-)}$ is the transverse displacement of the trajectory at the detector plane.

$L_{eff}(B)$ is defined as the ratio of the $\int Bdl$ along the trajectory to the field value as measured at the center of the magnet (B). $G(d_1, d_2)$ is a correction for the finite detector sizes. Both of these functions were extracted using TOSCA calculated field maps (due to the lack of detailed field measurements). $F(B)$ is an additional correction factor to account for differences between the real, and the calculated field distributions. In the ideal case of knowing the field distribution absolutely, $F(B) = 1$. As it will be shown below, using the simulated field, the accuracy of the approximation of Eq.(2) is better that the required accuracy for these measurements ($< 10^{-3}$).

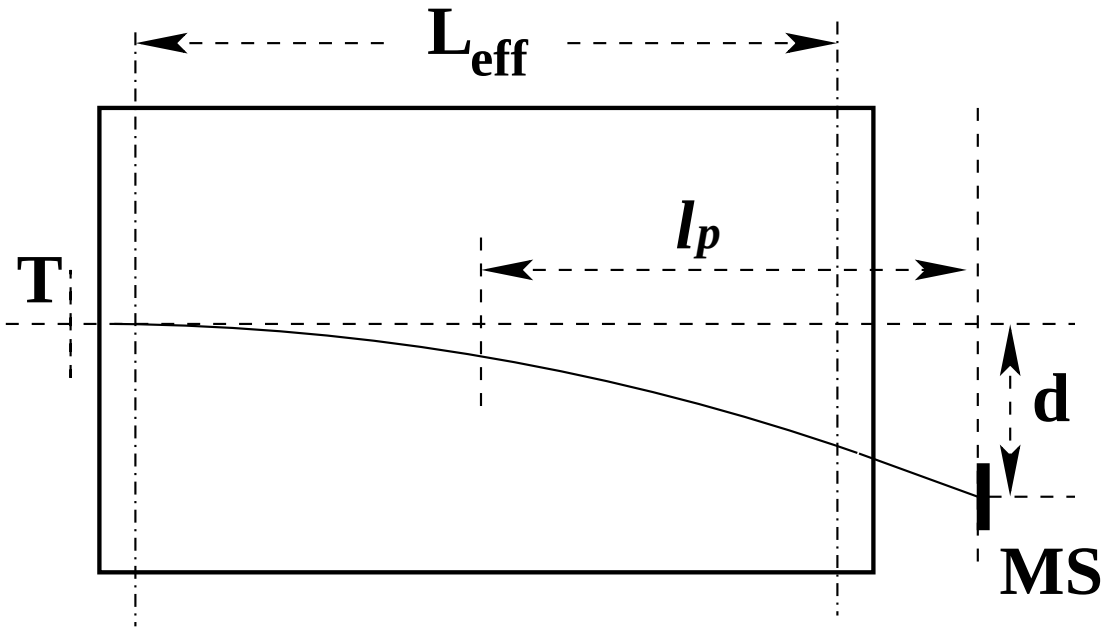

Figure 9: Schematics of the magnetic field model.

4.1 Determination of $L_{eff}(B)$ and $G(d_{e^+}, d_{e^-})$

If the field distribution is known, L_{eff} can be defined with sufficient accuracy using a simulation of the trajectories from the target to the detector. Unfortunately, the PS field maps have been measured along the direction of the beam (Z-axis) for a few settings of the magnet, and only for a few points in the transverse direction (X-axis): they are not covering the full transverse range of the setup used for this measurement.

The TOSCA model for the PS dipole [5] reproduces the field distribution in the homogeneous part of the magnet very well, but has small discrepancies in the fringe field region (see Figure 10). The overall difference between the generated and the real fields will be taken into account in $F(B)$. It should be noted that this difference effects mostly L_{eff}. The correction function G is not sensitive to the exact field distribution.

In Figure 11, the dependence of L_{eff} on B is shown. The integral is calculated along the central trajectory of the detector geometry. The simulation

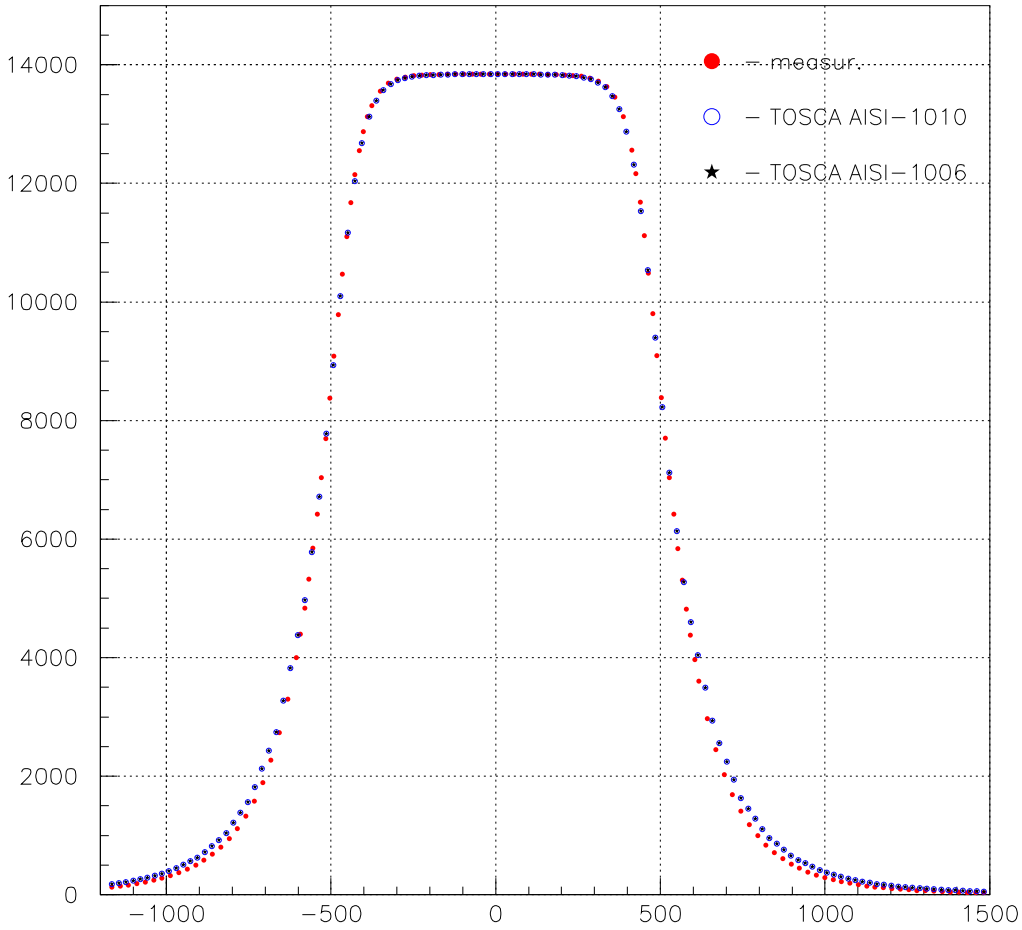

Figure 10: Comparison of the measured and TOSCA generated fields.

of the trajectories were done using Runge-Kutta-Nystroem method [6]. The points in Figure 11 are fitted with polynomial function:

$$L_{eff}(B) = P_0 + P_1 \cdot B + P_2 \cdot B^2 + P_3 \cdot B^3 \tag{4}$$

For the determination of the function $G(d_{e^+}, d_{e^-})$, pairs of trajectories were generated in a large momentum space to cover the full acceptance of the PS detectors. Simulations have been done for several PS field values, generating about 10^4 pairs for each setting. Transverse displacement of trajectories in the detector plane were used to calculate E_γ^c as defined in Eq.(2), without correction functions G and F. In Figure 12, the ratio of the gen-

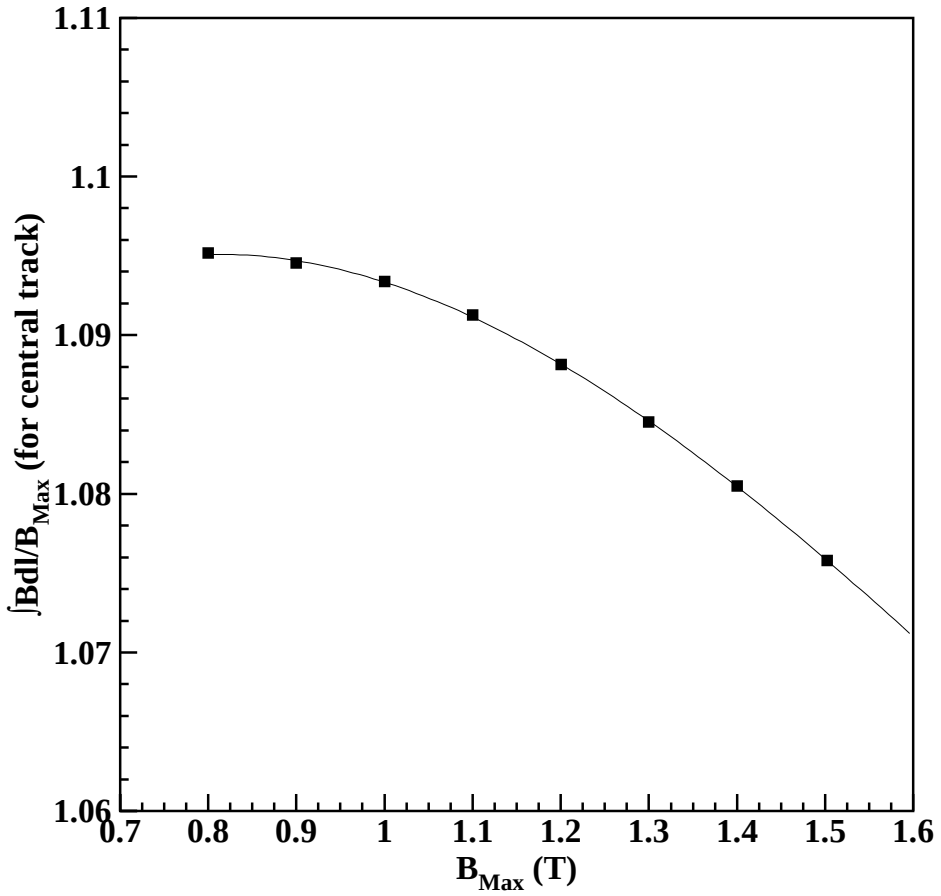

Figure 11: Dependence of L_{eff} on B_i.

erated photon energy, E_γ, to E_γ^c is shown as a function of the sum of the transverse displacement of the pair of trajectories (distance between e^+ and e^-) for the central field value $B_i = 0.3$T. An almost linear dependence is observed with very small variations ($< 0.3\%$) over the large range of distances. Note that the detector geometry selects distances from 43 to 47 cm. A third degree polynomial function is used to fit the dependence, $G(d_{e^+}, d_{e^-})$.

$$G(d_{e^+}, d_{e^-}) = P_0 + P_1 \cdot (d_{e^+} + d_{e^-}) + P_2 \cdot (d_{e^+} + d_{e^-})^2 + P_3 \cdot (d_{e^+} + d_{e^-})^3 \quad (5)$$

Similar dependences are obtained for several different field settings, covering the full range of the measurements. In Figure 13, the ratio for five

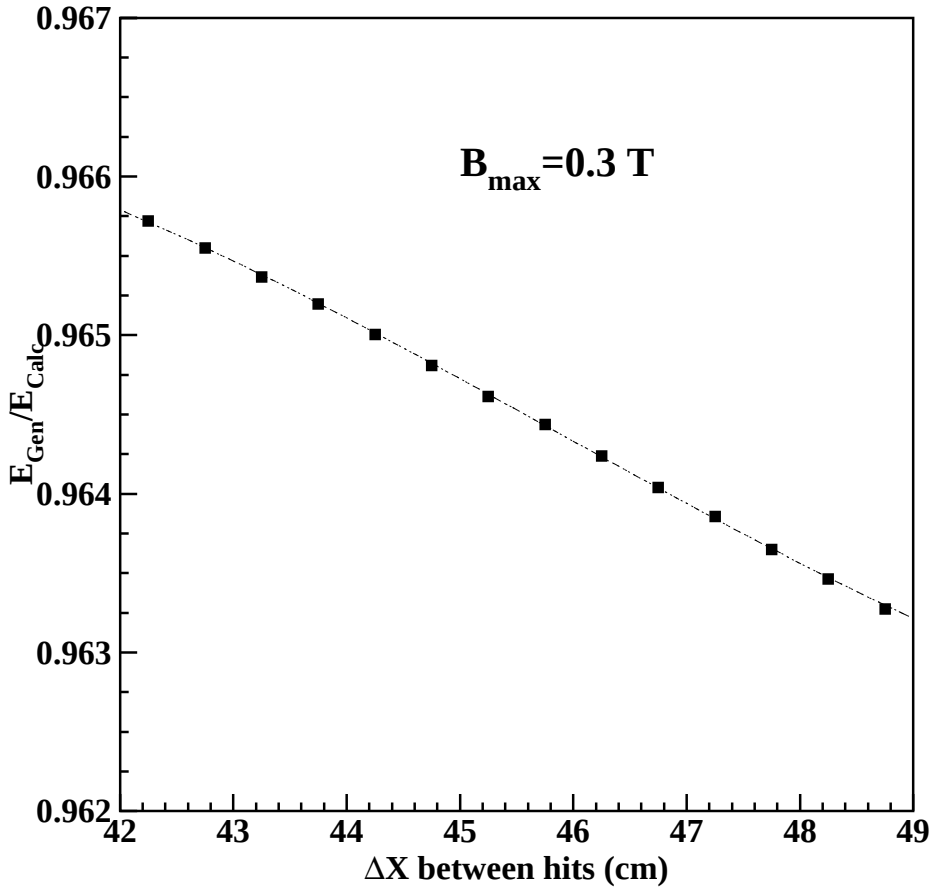

Figure 12: Dependence of the ratio of the simulated photon energy to the E_γ^c as defined in Eq.(2).

different field values (up to 1.5 T), scaled by the dependence obtained at 0.3 T, is presented. As one can see, $G(d_{e^+} + d_{e^-})$ found at 0.3 T describes the position dependence at all fields very well.

As was noted above, Figure 13 shows the validity of the approximation used in the calculation of the photon energy by Eq.(2). In the ideal case of accurate knowledge of the field distribution, Eq.(2) holds with an accuracy of better than 0.1%**.**

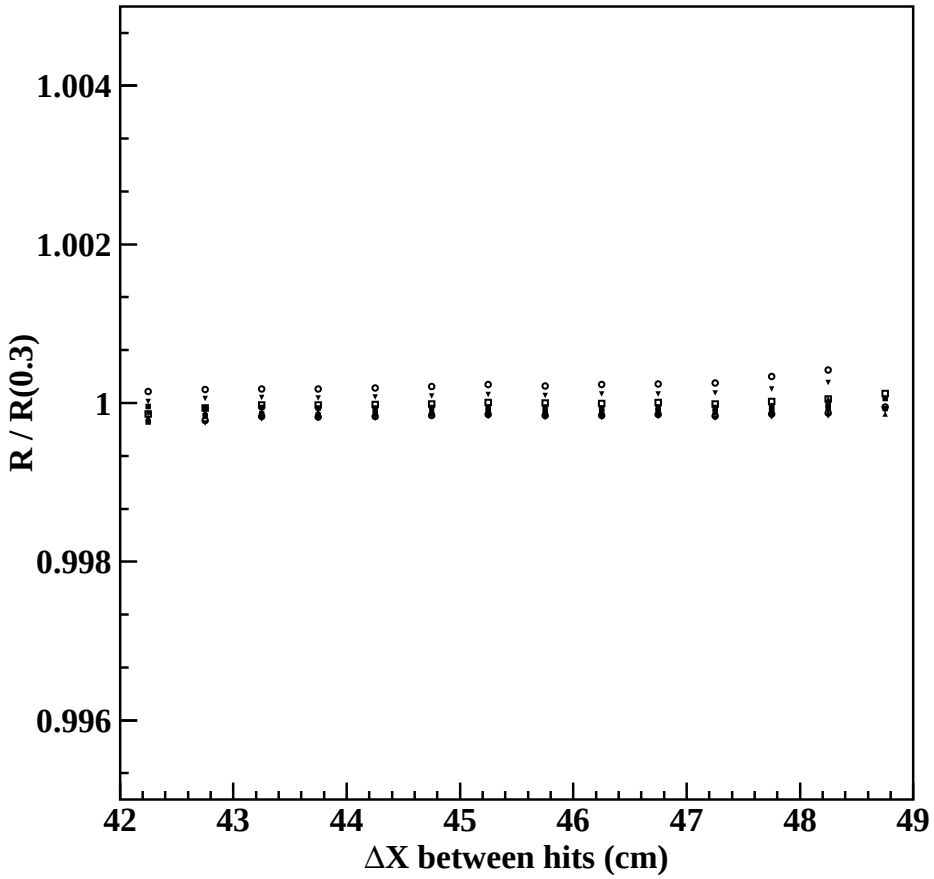

Figure 13: The ratio of the generated photon energy to the E_γ as defined in Eq.(2) for several central field values, scaled by the ratios at $B_i = 0.3$ T.

4.2 Determination of $F(B)$

The effective field length was calculated based on the TOSCA generated field map [5]. As described above, the generated and real field distributions are different (see Figure 10), and, therefore, another correction factor, $F(B)$, was introduced to account for this difference. To derive this correction, the $\int Bdl$ along the Z-axis for the measured and the TOSCA calculated field distributions were studied. *Integrals along the Z-axis are compared since there are not enough measured points to define the integral along the real trajectory, even for a single field setting.* The ratio of these integrals, $R = \int B_m dl / \int B_c dl$ was studied for four different transverse positions, $X = 0$ cm, $X = 8.5$ cm, $X = 13.6$ cm, and 18.7 cm. In Figure 14.a, the dependence of R on the field in the center of the magnet is shown. Due to lack of simulated field distributions at the exact X positions where the measurements were taken, B_c for $X = 8.5$ cm was taken to be the average of the fields at $X = 8$ cm and $X = 9$ cm. For the ratio at $X = 13.6$ cm, the average field value calculated at $X = 13$ cm and $X = 14$ cm is used, and for $X = 18.7$ cm, the calculated field at $X = 19$ cm is used. At $X = 8.5$ cm, $X = 13.6$ cm and 18.7 cm measurements are available for only five settings of the PS field. For the $X = 0$ point, the Z-dependence is measured at eight settings. It is clear from the figure that there is a strong dependence of R on B-value, $F(B)$. This dependence reflects the fact that in the calculation, the shape of $B(z)$ is independent of B (it scales at all values of Z), while in reality the fringe field changes with field settings. In Figure 15, the distribution of the ratio of the measured fields at different central values to the setting with central field value of 0.8 T is shown as a function of Z. One can clearly see the non-constant behavior in the fringe field region.

In Figure 14.a, the absolute scale depends on X, but the shape is similar for all X values. Since for real trajectories, the integral covers large range of X, and the absolute energy scale will be defined by the "end point" measurements, the absolute scale is not important. For the analysis, the shape of the dependence of R on the field value at $X = 0$ is used, $F(B) = R(0)$. The uncertainty in the determination of the $F(B)$ is the largest contribution to the error in the final corrections. The estimated error in $F(B)$ is $\pm 0.05\%$, based on the variations of $R/F(B)$ for single X, see Figure 14.b.

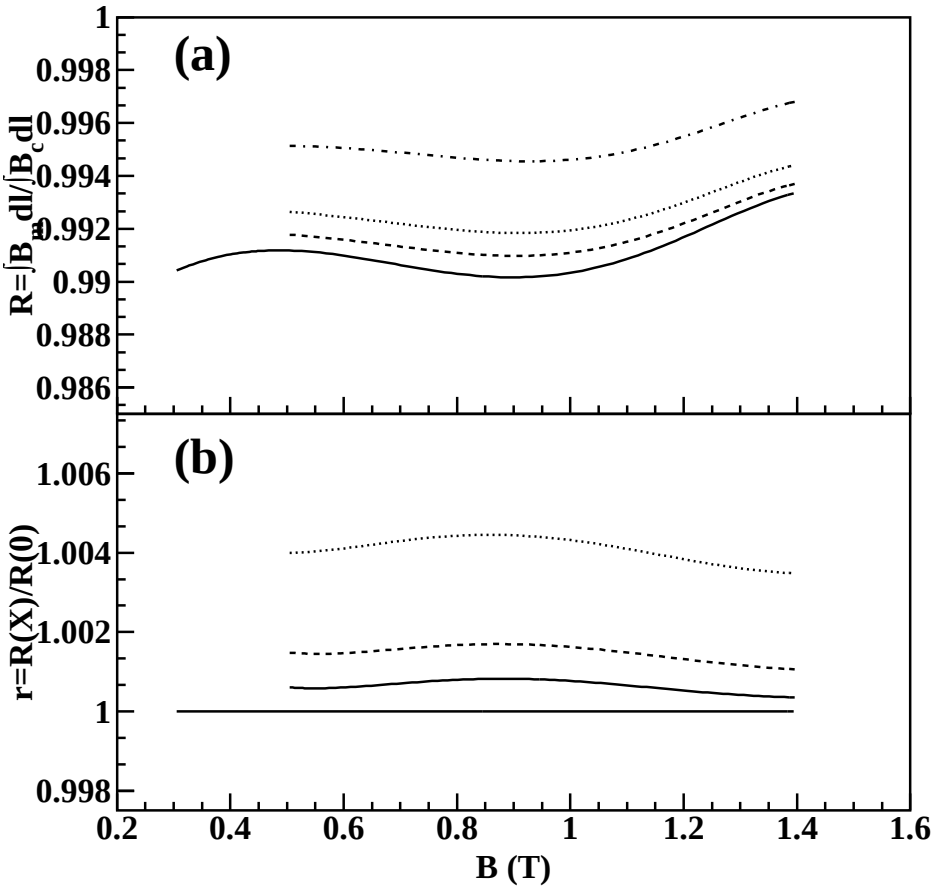

Figure 14: Comparison of $\int Bdl$ values along the Z axis, calculated using the measured and the TOSCA calculated field distributions. (a) - the ratio of integrals at different distances from the magnet centerline: the solid line at $X = 0$, the dashed line at $X = 8.5$ cm, the dotted line at $X = 13.6$ cm, and the dashed-dotted line at $X = 18.6$ cm. (b) - the same ratios normalized to the ratio at $X = 0$.

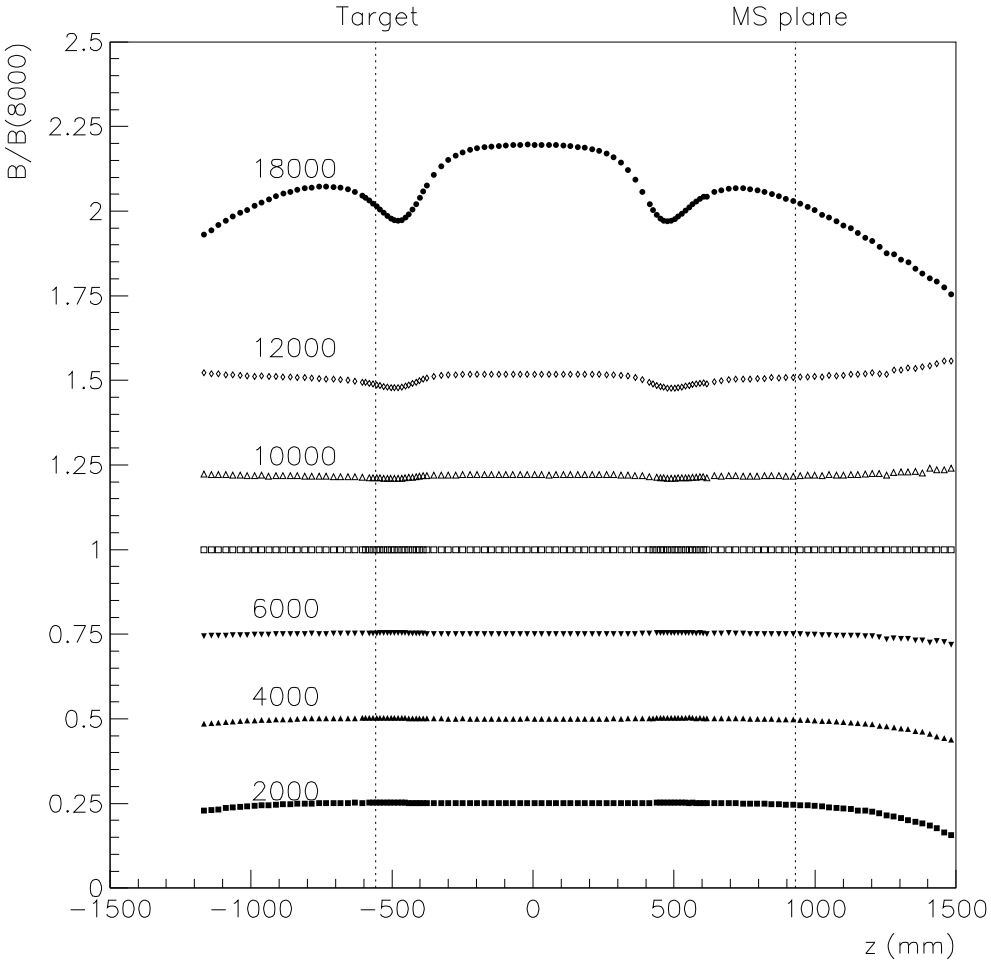

Figure 15: Ratio of the the measured fields at different setting to the measured field at 0.8 T as function of Z

4.3 Determination of C_i constants

In Figure 16, the distributions of the ratio E_c/E^i_{tagg} are shown for E-counters $i = 76,\ 149,\ 391$ and 576. Similar distributions have been analyzed for all E-counters. Events from different runs at different PS field settings are contributing to the distribution of every E-counter (see Figure 3). The correction factor C_i for the E-counter "i" is defined as the mean of the distribution. To determine the mean, a fit to the distributions of ratios is done using a function that is a sum of two Gaussians and a linear function. In Figure 16, the fit results are shown by the red lines. The parameter $P2$ (mean of the narrow Gaussian) is taken as C_i.

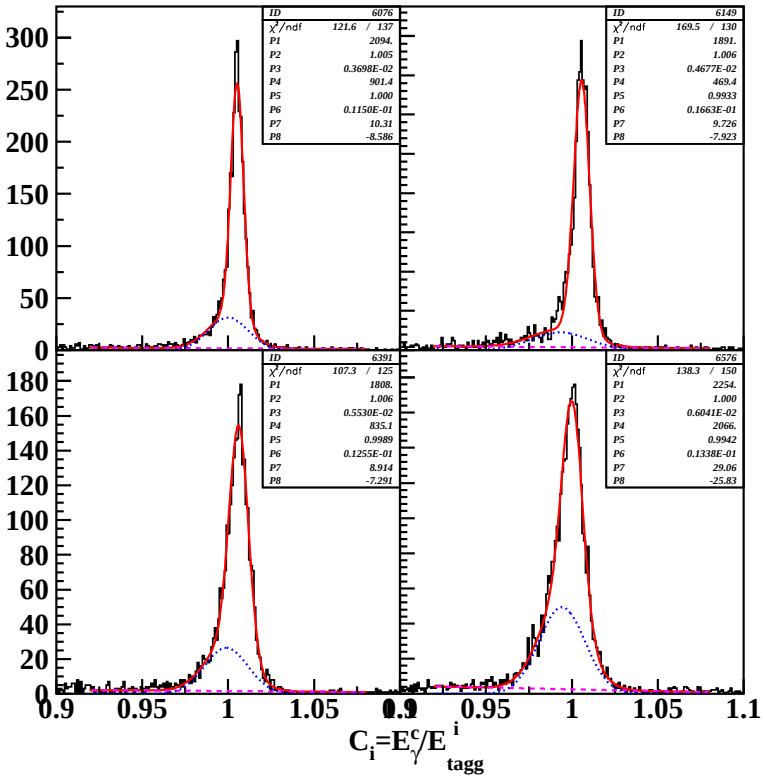

Figure 16: Fit to the C_i distributions of E-counters #76, 149, 391, and 576. As a fit function a sum of two Gaussian and a linear function is used. The fit parameter $P2$ corresponds to C_i.

5 End-point measurements

For a given detector acceptance, with an increase of the B-field one effectively selects e^+e^- pairs from higher energy photons, and at some point will reach the "end-point energy", E_0. Measurements of the e^+e^- coincidence rate as a function of the B-field value, at fixed geometry, allow one to relate the B-field value to the maximum energy of the photon beam, E_0.

The e^+e^- coincidence rate was studied for several different detector geometries (different regions of X planes). In Figure 17, the e^+e^- coincidence rate is plotted as a function of photon energy as defined in Eq.(2). Data obtained at the PS dipole field values from 1.9T to -1.35T are combined. The vertical line passes through the middle of the falling edge, and corresponds to the energy of $E_B = 3.784$ GeV. The beam energy for these measurements was $E_0 = 3.7765$ GeV (based on energy measurements done in Hall A, and in the accelerator). A constant $\eta = E_0/E_B = 0.9985$ was found for the correction of the energy scale in Eq.(2) for the geometry setting that was used to derive the corrections C_i.

6 Final corrections

The final tagger energy corrections were computed using the C_i constants for each E-counter and the energy scale correction factor η. In Figure 18, the final corrections are plotted as function of the E-counter ID. A few outlying points around the counters 120 and 440 are due to mis-cabling (this was found and fixed). The estimated errors of these correction constants is about $\pm 0.1\%$, and is defined largely by the determination of $F(B)$. Corrections for counters with ID > 700 have much larger errors due to the PS resolution and the limited statistics. The table for use in the data analysis is in \$CLAS_PARMS/g10_PS_measured_taggEcorr.dat. The format is: E-counter ID, correction C_i, fit error for C_i, width (σ) of the distribution E_c/E^i_{tagg}, fit error for the width.

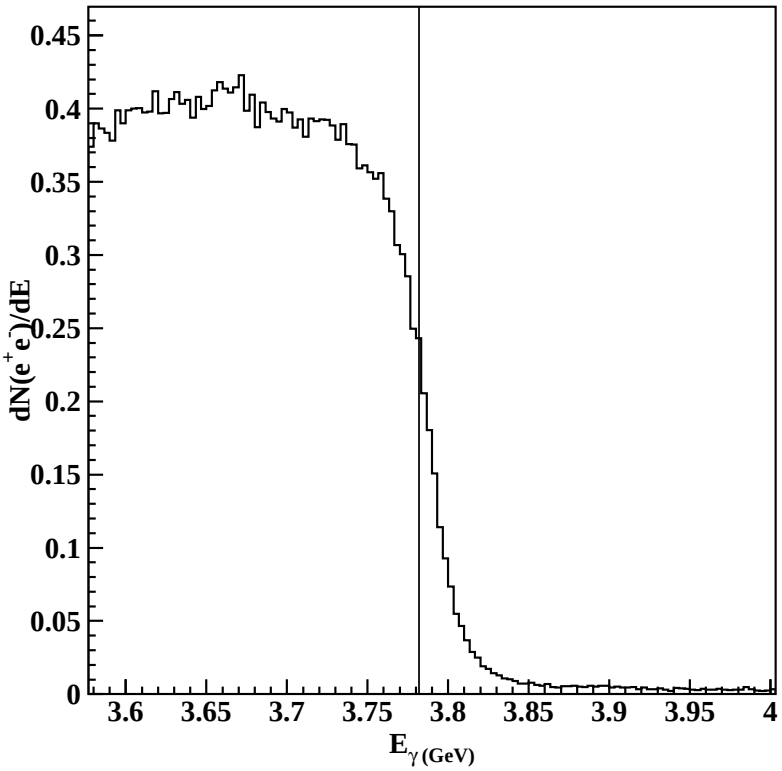

Figure 17: The e^+e^- coincidence rate as a function of energy calculated using the Eq.(2). Vertical line passes through the mid point of the falling edge, and is at $E = 3.782$ GeV.

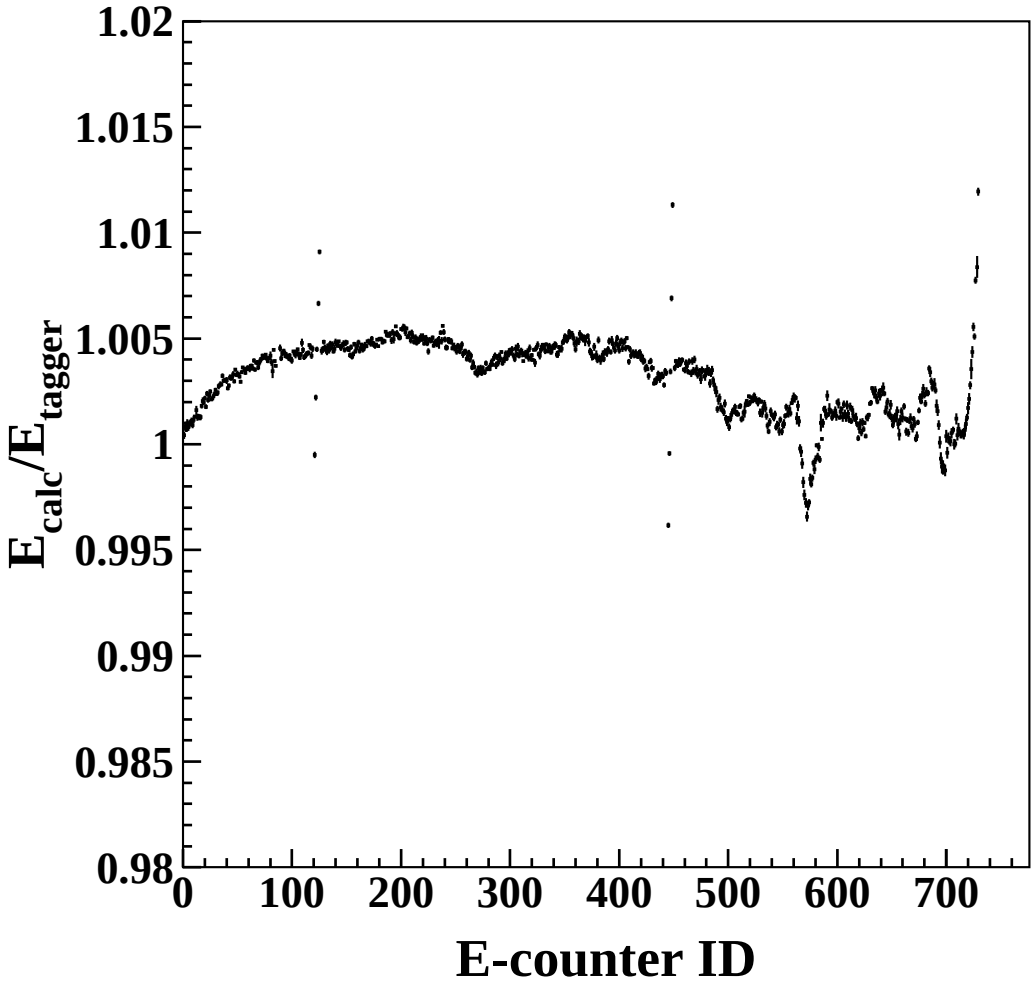

Figure 18: The final tagger energy corrections for `g10` (`g11`) run periods.

References

[1] D.I. Sober et al., NIM **A440**, (2000) 263-284.

[2] D.I. Sober, H. Crannell and and F.J. Klein, CLAS-NOTE 2004-019.

[3] S. Stepanyan; CLAS-ANALYSIS 2003-105.

[4] D. Dale "http://www.pa.uky.edu/ dale/".

[5] A. Glamazdin, TOSCA simulation of the Hall B pair spectrometer dipole field.

[6] FORTRAN code from B. Mecking.